CHAPTER 5

CONTROLLER DESIGNS

5.1 Introduction

For the design of the diagonal controllers Bode and root locus plots as well as time domain simulations served as an indication of controller performance. In the design of the H_∞ controllers singular value plots of the sensitivity and complementary sensitivity transfer function together with singular value plots of the performance and robustness bounds respectively, are used as an indication of the performance of the H_∞ controllers. In addition to frequency domain plots, closed-loop time domain simulations were used as a check on the H_∞ controller behaviour. This chapter also gives some necessary specifications of the controller as well as the values that were used for their tuning parameters. Starting with the specifications in section 5.2, a brief discussion of the diagonal controllers design follows in section 5.3. In sections 5.4 and 5.5 the H_∞ controller designs for the LTI models in sections 3.4.2 and 3.4.3 respectively are given. Lastly in section 5.6 a comparison of the diagonal and H_∞ controllers is done by means of singular value plots of their closed loop transfer functions and also by means of time domain simulations.

5.2 Controller Specifications

Controller specifications are given in terms of the following requirements:

i) Exit gauge is to be kept within 1% of its setup value in the presence of control error changes [41].

ii) Front and back tensions are to be kept within 40% of their setup values [41].

iii) Control actions are to be kept within realistic limits, i.e. $|x_{sp}| = |u_1| \leq 6.5 \cdot 10^{-3}$ m, $|\dot{v}_{bc}| = |\dot{u}_2| \leq 21$ m/s^2 and $|\dot{v}_{fc}| = |\dot{u}_2| \leq 120$ m/s^2 (see App.B).

iv) Nominal stability is to be guaranteed.

5.3 Diagonal Controller Design

The parameters of the diagonal controller $K_{diag}(s)$,

$$K_{diag}(s) = \begin{bmatrix} k_{11}(s) & 0 & 0 \\ 0 & k_{22}(s) & 0 \\ 0 & 0 & k_{33}(s) \end{bmatrix} \tag{5.1}$$

were obtained by using the methods described in section 4.1.

The main reason for the design of a diagonal controller is to try the simplest controller first. Furthermore two arguments have relevance in the decision on a diagonal controller design. The first one is that for the maximum step sizes of coiler speed and actuator stroke, the influence of the coiler speed step on strip exit gauge is by two orders of magnitude smaller than that of the direct input, hydraulic actuator stroke. Another argument, which supported the choice for a diagonal controller scheme is that the frequency of the variations on the plant output, exit gauge, is less than its SISO closed-loop bandwidth. These variations in exit gauge are a result of tension variations and can be regarded as disturbances because of their frequency being lower than the corresponding closed-loop bandwidth. The bandwidths of the transfer functions on the diagonal of the first linear model in closed loop with their corresponding controllers can be obtained from the Bode plots in figures 5.1 through 5.3 at the frequency where the log magnitude curve crosses the –3 decibel line. The frequency of the gauge/tension interaction is approximately 1.34 rad/s, which is lower than the bandwidths of these transfer functions on the diagonal in closed loop with their controllers.

Table 5.1: Closed loop bandwidths of transfer functions on the diagonal

Transfer function	Closed loop bandwidth [rad/s]
$g_{11}(s)$	2
$g_{22}(s)$	90
$g_{33}(s)$	90

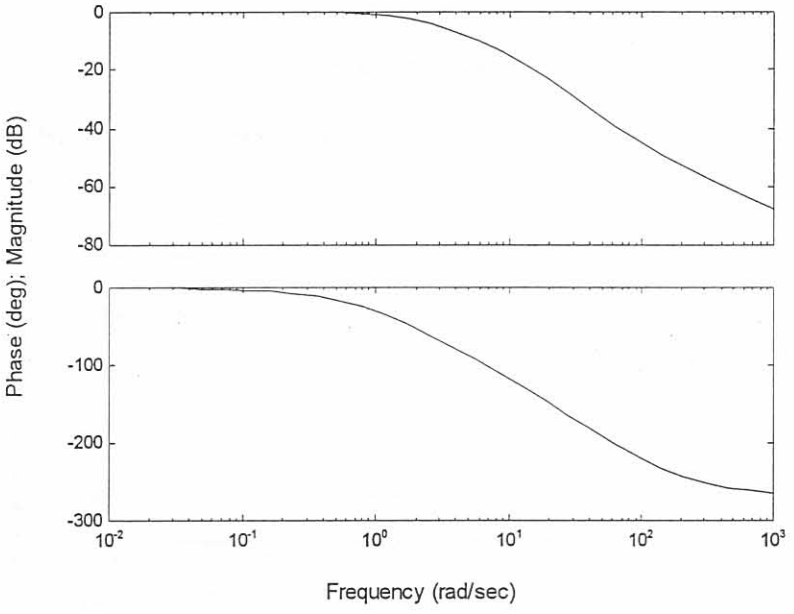

Figure 5.1: Bode plot of $g_{11}(s)$ of first linear model in closed loop with PID control.

The PID controller $k_{11}(s)$ was designed as SISO controller for the plant represented by the transfer function Eq. 3.4. The tuning parameters obtained for this design were $\alpha_1 = 0.55$ and $\alpha_2 = 0.03$. Speed of response of the closed loop had to be traded off against control action changes, which needed to be within realistic limits. Overshoot and bandwidth of this SISO system can be influenced by adjusting only α_1 and α_2, since the PID gains (equations 4.9 through 4.11) are given directly in terms of the model parameters in Eq. 4.2 and the design filter in Eq. 4.6 [34].

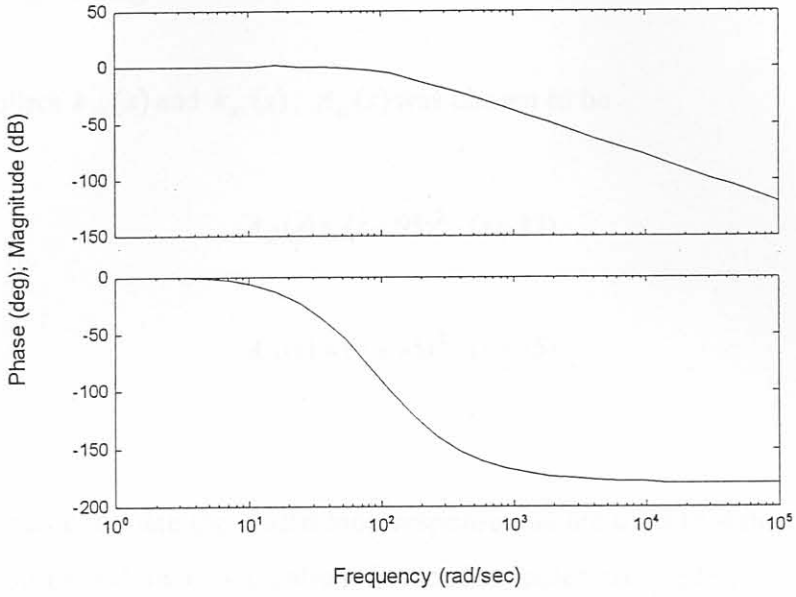

Figure 5.2: Bode plot of $g_{22}(s)$ of first linear model in closed loop with PI control.

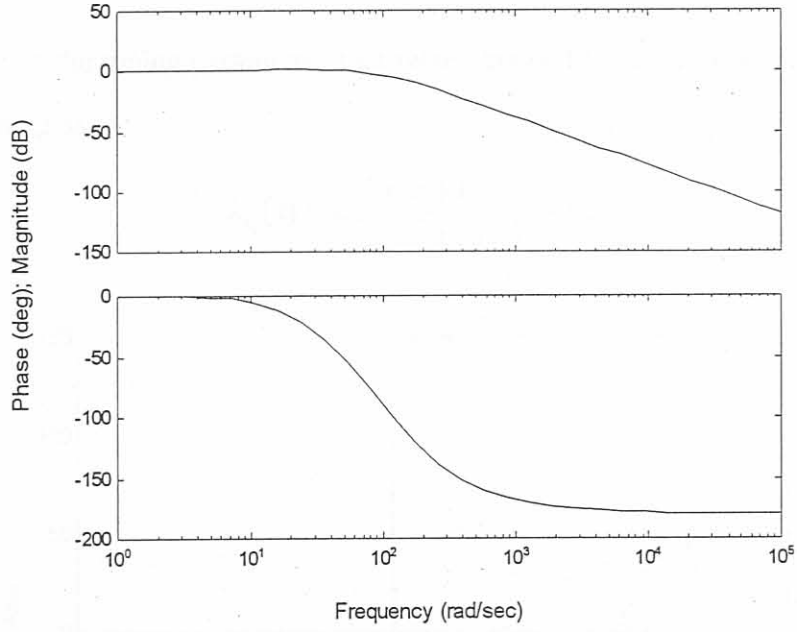

Figure 5.3: Bode plot of $g_{33}(s)$ of first linear model in closed loop with PI control.

PI control is used for $k_{22}(s)$ and $k_{33}(s)$, because it is a popular controller [36]. Integral control on its own would result in persistent oscillation. However some damping is produced with the addition of proportional control. By means of the chosen design method, pole placement design, proper tuning is available and oscillations that can accompany the use of PI controllers [36] are avoided. The root locus plots figures 5.4 and

5.5 indicate the tendency of the closed loops with PI controllers to oscillate with two branches leaving the negative real axis.

For PI controllers $k_{22}(s)$ and $k_{33}(s)$, $A_{cl}(s)$ was chosen to be

$$A_{cl}(s) = (s+95)^2 \cdot (s+12) \tag{5.3}$$

and

$$A_{cl}(s) = (s+95)^2 \cdot (s+15) \tag{5.4}$$

respectively.

The slower poles dominate the closed loop response and are used to influence overshoot in the closed loop time domain simulation. If the slow poles are made less negative it helps to reduce overshoot. The purpose of the fast poles, in $A_{cl}(s)$, is to give a fast response, i.e. a large bandwidth, of the closed SISO loops.

Table 5.2 shows the tuning parameters that were obtained for controllers $k_{22}(s)$ and $k_{33}(s)$ with the meaning as in

$$k_{ii}(s) = \kappa_c \left(\frac{\tau_I s + 1}{\tau_I s} \right) \quad , \; i \in [2,3] \tag{5.5}$$

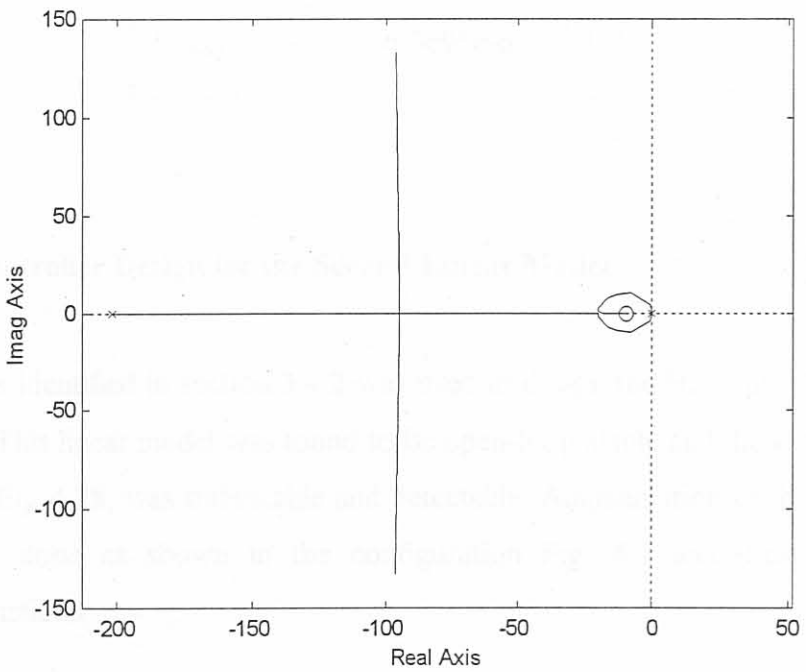

Figure 5.4: Root locus of $g_{22}(s)$ of first linear model in closed loop with PI control.

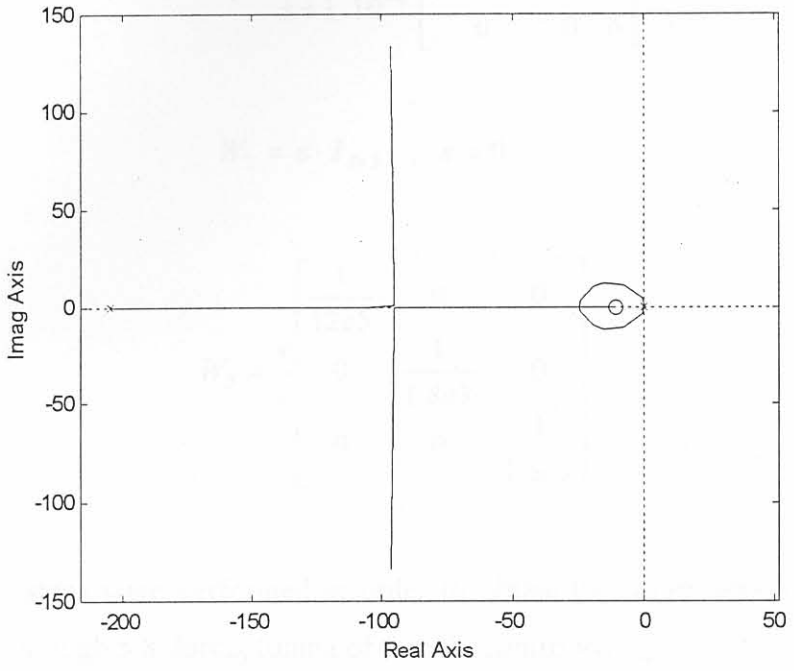

Figure 5.5: Root locus of $g_{33}(s)$ of first linear model in closed loop with PI control.

Table 5.2: Tuning parameters for $k_{22}(s)$ and $k_{33}(s)$

Controller	κ_c	τ_I
$k_{22}(s)$	-3.7129e-6	1.0
$k_{33}(s)$	6.0695e-6	1.0

5.4 H_∞ Controller Design for the Second Linear Model

The model as identified in section 3.4.2 was used to design the H_∞ controller discussed in this section. This linear model was found to be open-loop stable and therefore the plant, as described in Eq. 4.28, was stabilizable and detectable. Augmentation of the linear plant by weights was done as shown in the configuration Fig. 4.4 and using the following weighting functions.

$$W_1 = \frac{0.2}{s+1\cdot 10^{-6}}\begin{bmatrix} 0.5e-4 & 0 & 0 \\ 0 & 6 & 0 \\ 0 & 0 & 6 \end{bmatrix} \tag{5.6}$$

$$W_2 = \varepsilon \cdot \boldsymbol{I}_{3\times 3} \quad ; \quad \varepsilon = 0 \tag{5.7}$$

$$W_3 = \frac{s}{1}\begin{bmatrix} \frac{1}{12e5} & 0 & 0 \\ 0 & \frac{1}{1.8e3} & 0 \\ 0 & 0 & \frac{1}{1.8e3} \end{bmatrix} \tag{5.8}$$

The following steps were performed in order to obtain the parameters in the weights of equations 5.6 through 5.8 during tuning of the H_∞ controller.

1. Adjust parameters in positions (2,2) and (3,3) of $W_1(s)$ in order to affect the speed of response. In this step it was found that a large difference between the values of the elements of $W_1(s)$ caused the performance bound to be violated.
2. Adjust parameter in position (1,1) of $W_3(s)$ in order to meet the performance bound specification, Eq. 4.26, if it has been violated in step 1. Decreasing of element (1,1) of $W_3(s)$ was done until control action, u_1, exceeded the limit specified in 5.2 iii).
3. If necessary, the gain of $W_1(s)$ needs to be adjusted such that the controller's performance for output y_1 is the same as that of the diagonal controller. If the performance of the controller with respect to outputs y_2 and y_3 deteriorated, steps 1 and 2 were repeated.

Figures 5.6 and 5.7 show how the closed loop meets the performance and robustness bound specifications respectively as given in equations 4.26 and 4.27.

The continuous state space matrices of the model-reduced form of this controller is given in App. C.1.

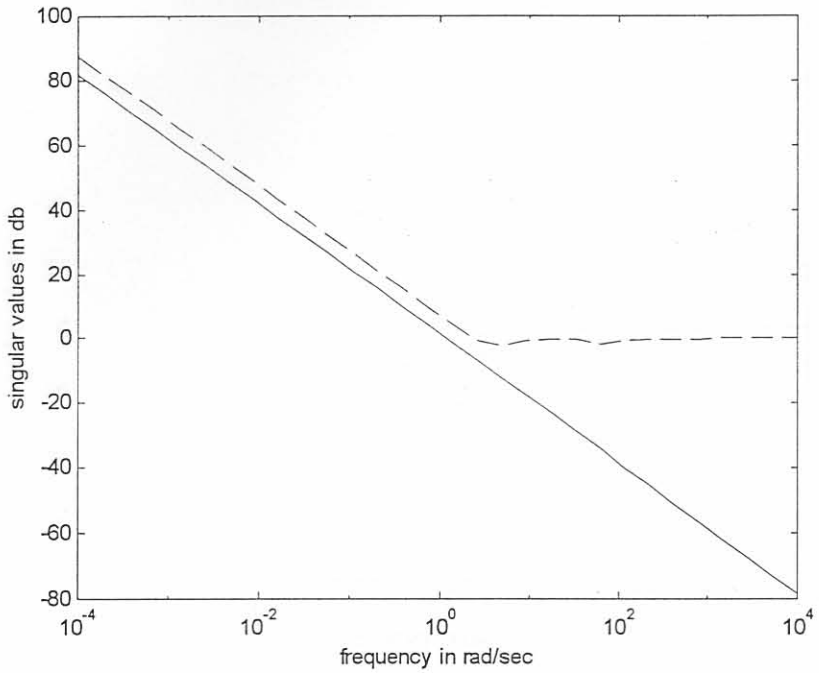

Figure 5.6: Plots of $1/\overline{\sigma}(S)$ (dashed line) and $\overline{\sigma}(W_1)$ (solid line) of second linear model in closed loop with its corresponding H_∞ controller.

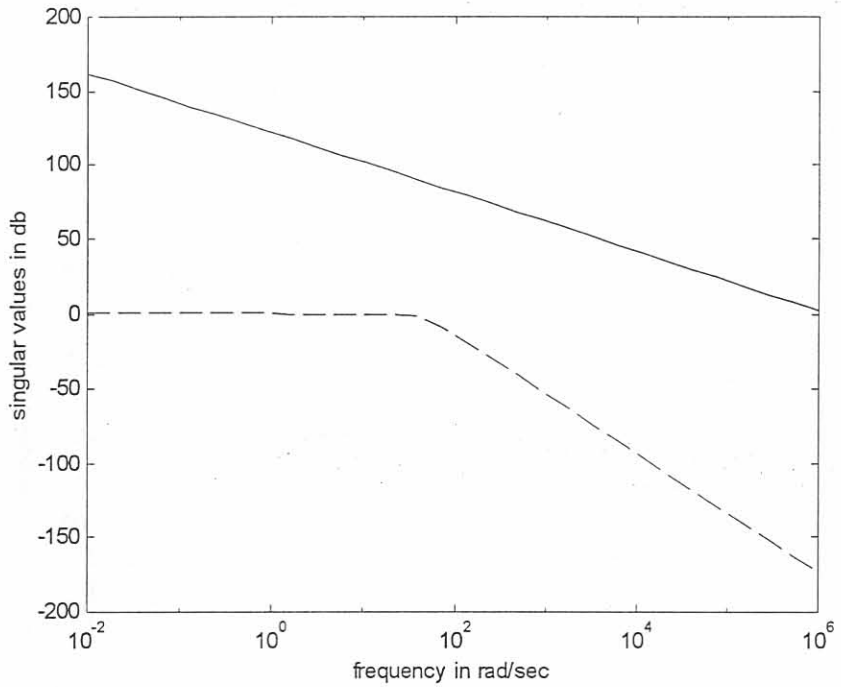

Figure 5.7: Plots of $\overline{\sigma}(T)$ (dashed line) and $\overline{\sigma}(W_3^{-1})$ (solid line) of second linear model in closed loop with its corresponding H_∞ controller.

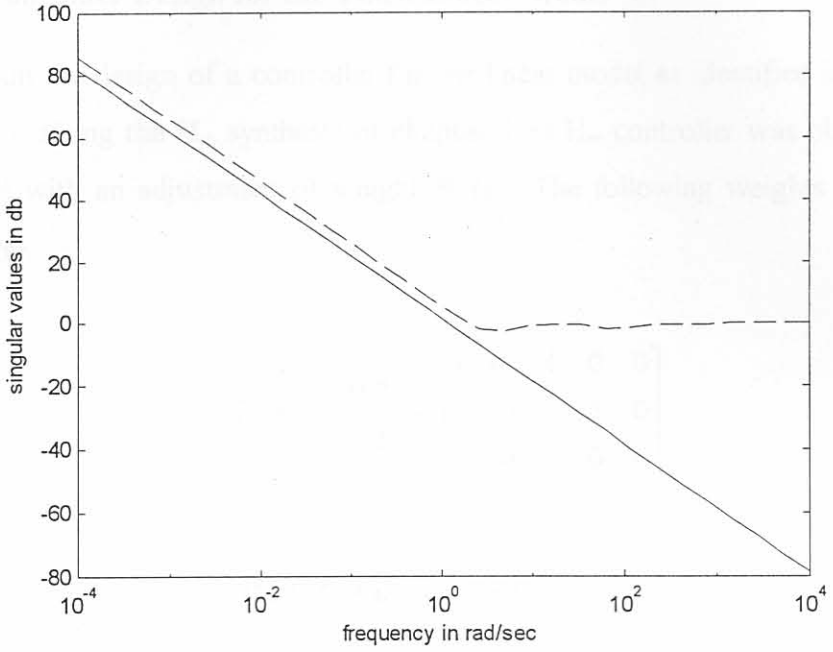

Figure 5.8: Plots of $1/\overline{\sigma}(S)$ (dashed line) and $\overline{\sigma}(W_1)$ (solid line) of third linear model in closed loop with its corresponding H_∞ controller.

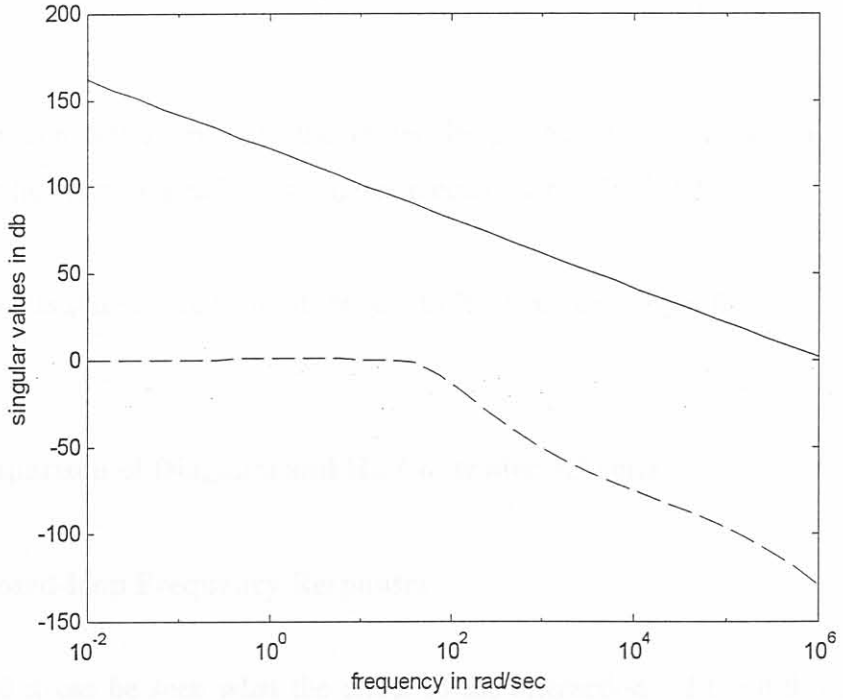

Figure 5.9: Plots of $\overline{\sigma}(T)$ (dashed line) and $\overline{\sigma}(W_3^{-1})$ (solid line) of third linear model in closed loop with its corresponding H_∞ controller.

5.5 H_∞ Controller Design for the Third Linear Model

In this section the design of a controller for the linear model as identified in section 3.4.3 is considered. Using the H_∞ synthesis of chapter 4 an H_∞ controller was obtained for this linear model with an adjustment of weight $W_1(s)$. The following weights were used for this controller.

$$W_1 = \frac{0.2}{s+1\cdot 10^{-6}}\begin{bmatrix} 0.4e-4 & 0 & 0 \\ 0 & 6 & 0 \\ 0 & 0 & 6 \end{bmatrix} \tag{5.6}$$

$$W_2 = \varepsilon \cdot I_{3\times 3} \quad ; \quad \varepsilon = 0 \tag{5.7}$$

$$W_3 = \frac{s}{1}\begin{bmatrix} \frac{1}{12e5} & 0 & 0 \\ 0 & \frac{1}{1.8e3} & 0 \\ 0 & 0 & \frac{1}{1.8e3} \end{bmatrix} \tag{5.8}$$

Figures 5.8 and 5.9 show how the closed loop meets the performance and robustness bound specifications respectively as given in equations 4.26 and 4.27.

The continuous state space form of this controller is given in App. C.2.

5.6 Comparison of Diagonal and H_∞ Controller Schemes

5.6.1 Closed-loop Frequency Responses

In Fig. 5.10 it can be seen what the effect of the interactions of the full first linear model are on the closed loop. The difference in maximum and minimum singular values of the diagonal controller in closed loop with the full first linear model is large compared to

corresponding quantities of the other two closed loop control systems. This is so because the interactions have not been accounted for in the design of the diagonal controller.

In closed loop with LTI models consisting of only the transfer functions on the diagonal, the diagonal and H_∞ controllers have a flat closed-loop frequency response for frequencies below 2 rad/s, which is desirable for good set point following and good disturbance rejection.

The effect of interactions can again be seen in Fig. 5.11, which compares the singular value plots of the closed-loop transfer function matrices of the H_∞ controllers for the second and third LTI models. The effect here is that the difference between maximum and minimum singular values becomes larger for higher frequencies.

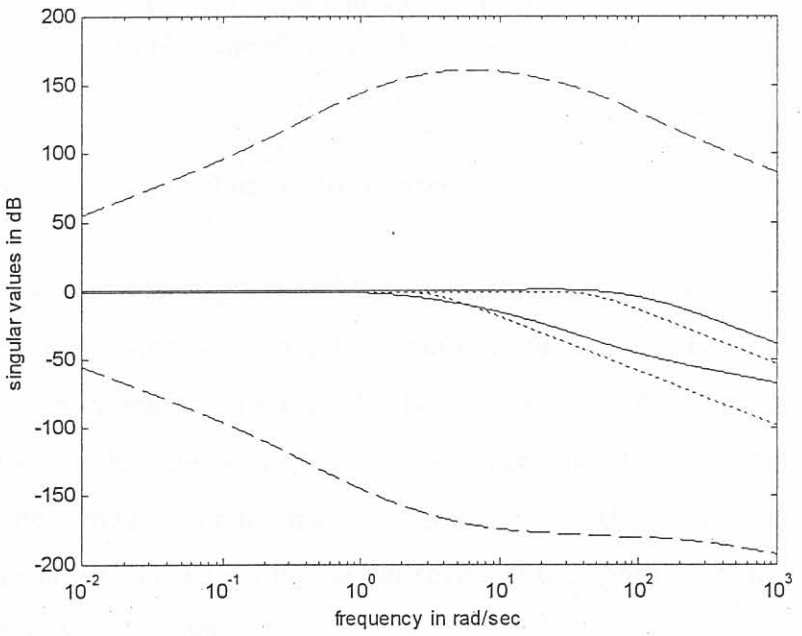

Figure 5.10: Maximum and minimum singular values of closed loop transfer functions of
i) diagonal controller with full first linear model (dashed),
ii) diagonal controller with diagonal first linear model (solid),
iii) H_∞ controller with second linear model (dotted).

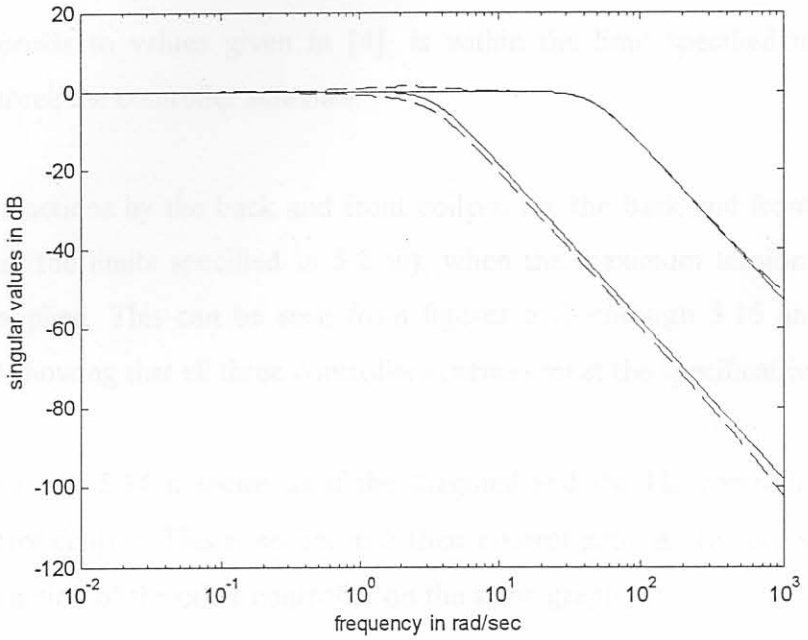

Figure 5.11: Maximum and minimum singular values of closed loop transfer functions of
i) H_∞ controller with second linear model (solid),
ii) H_∞ controller with third linear model (dashed).

5.6.2 Closed-loop Time Domain Responses

Fig. 5.12 shows that the diagonal and the H_∞ controller in closed loop with the first and second LTI model respectively have been tuned to have the same settling times for exit gauge. As shown in figures 5.13 and 5.14 the settling times for the tensions in the case of the diagonal controller scheme are 0.2 seconds longer than those of the H_∞ controller for the second linear model. For the matter of comparing both the latter controller schemes this difference in tension settling time is not severe in the light of the total settling time for exit gauge, which is 2.5 seconds.

Comparing the performance of the H_∞ controllers for the second and third LTI models no difference in settling times of the controlled variables can be found as shown in figures 5.17 through 5.19.

In the diagonal controller scheme the integrator parts of its individual controller transfer functions help to achieve specification i) and ii). So does the weight, $W_1(s)$, with its integrator characteristics in the H_∞ controllers for the second and third linear models.

The controller action, u_1, i.e. hydraulic actuator stroke, for set point changes in exit gauge, which corresponds to values given in [4], is within the limit specified in 5.2 iii). This applies to all three the controller schemes.

The controller actions by the back and front coilers, i.e. the back and front coiler speeds, are also within the limits specified in 5.2 iii), when the maximum tension step set point changes are applied. This can be seen from figures 5.13 through 5.16 and from figures 5.18 and 5.19 showing that all three controller schemes meet the specification 5.2 iii).

In figures 5.13 and 5.14 it seems as if the diagonal and the H_∞ controllers respectively apply no control actions. This is so because their control actions are very small compared to the control action of the other controller on the same graph.

The fact that for the closed loops for all three controller schemes and their corresponding LTI plant models, the poles are in the open left half s-plane shows that specification iv) is satisfied by all three systems.

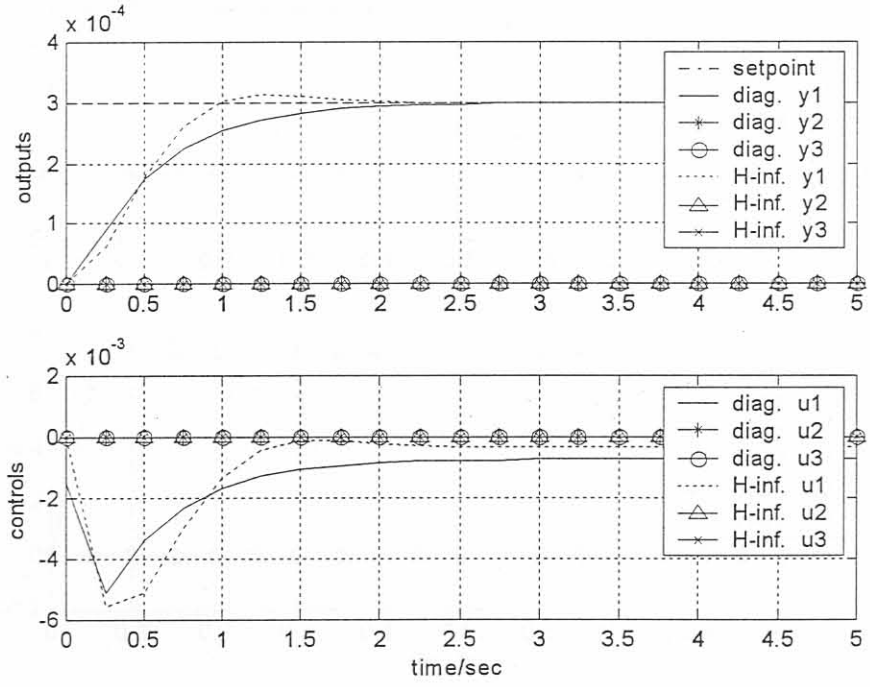

Figure 5.12: Closed loop simulation results of the diagonal controller with the diagonal first linear model and an H_∞ controller with the second linear model for the set point r = [3e-4 0 0] – (SI units apply).

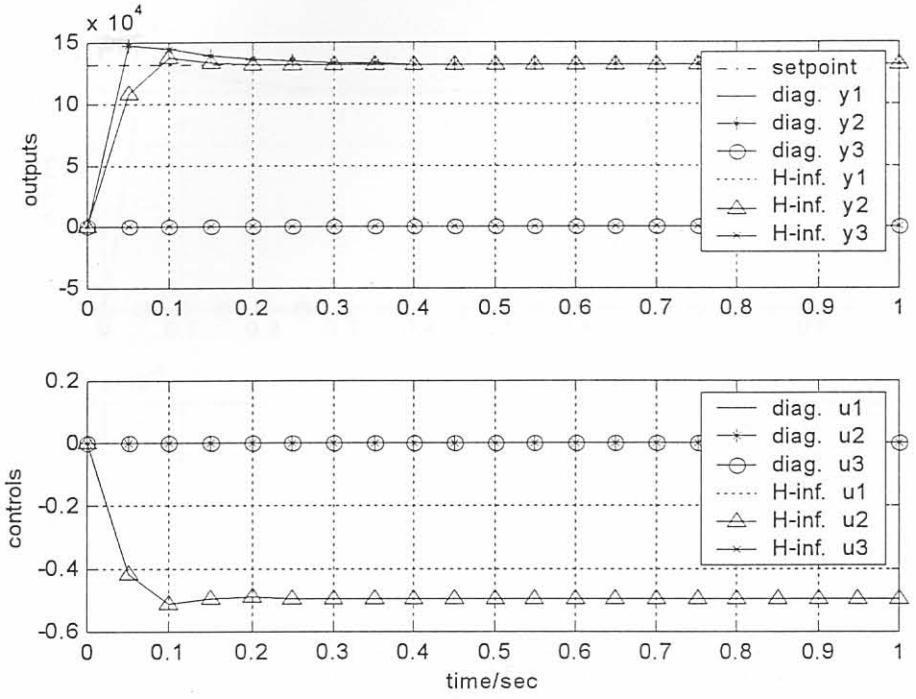

Figure 5.13: Closed loop simulation results of the diagonal controller with the diagonal first linear model and an H_∞ controller with the second linear model for the set point r = [0 1.32e5 0] – (SI units apply).

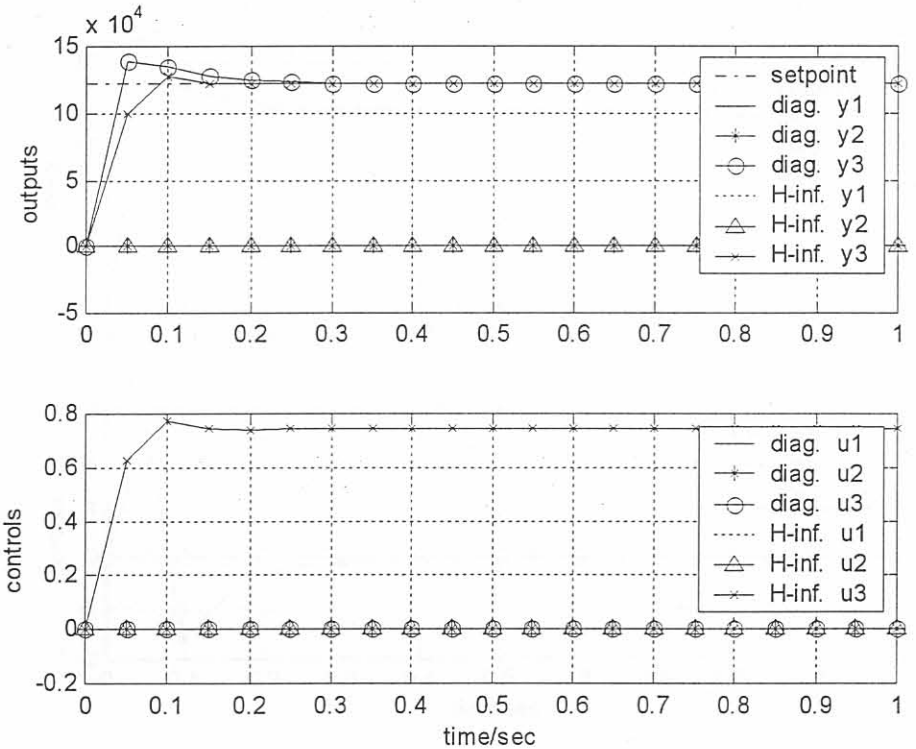

Figure 5.14: Closed loop simulation results of the diagonal controller with the diagonal first linear model and an H_∞ controller with the second linear model for the set point r = [0 0 1.22e5] – (SI units apply).

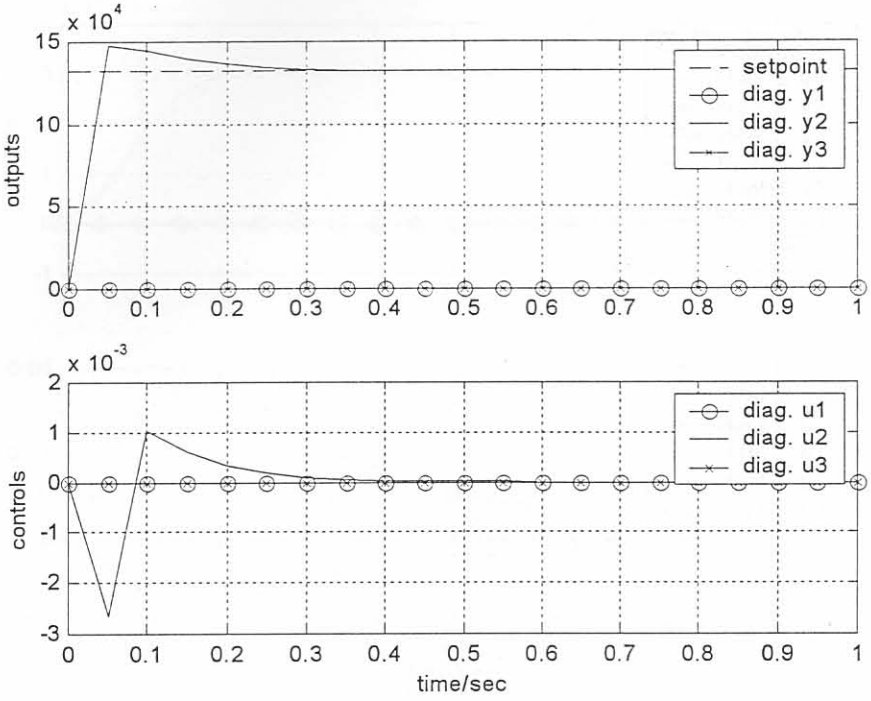

Figure 5.15: Closed loop simulation results of the diagonal controller with the diagonal first linear model for the set point r = [0 1.32e5 0] – (SI units apply).

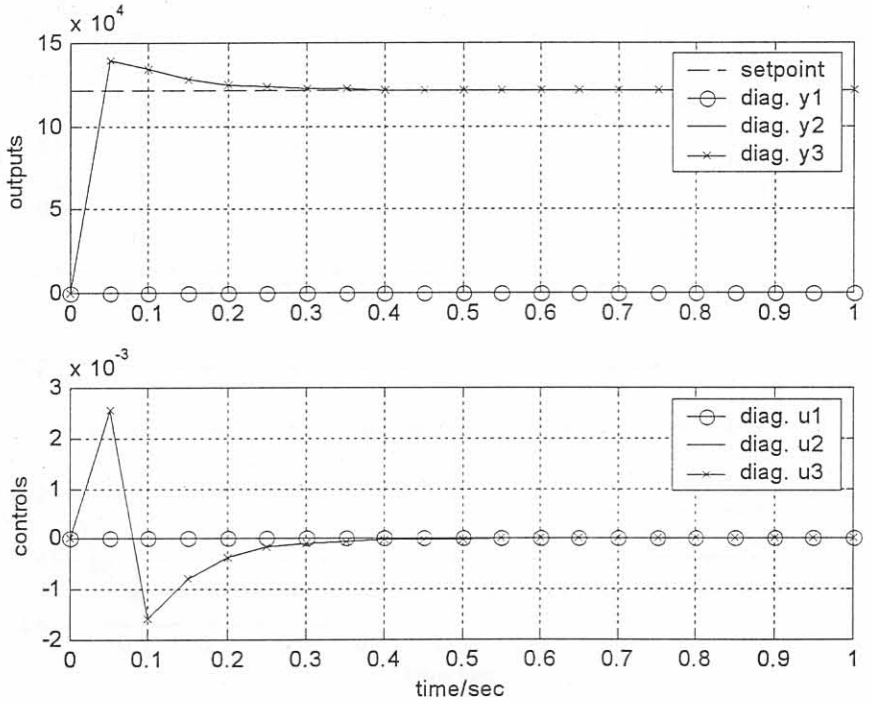

Figure 5.16: Closed loop simulation results of the diagonal controller with the diagonal first linear model for the set point r = [0 0 1.22e5] – (SI units apply).

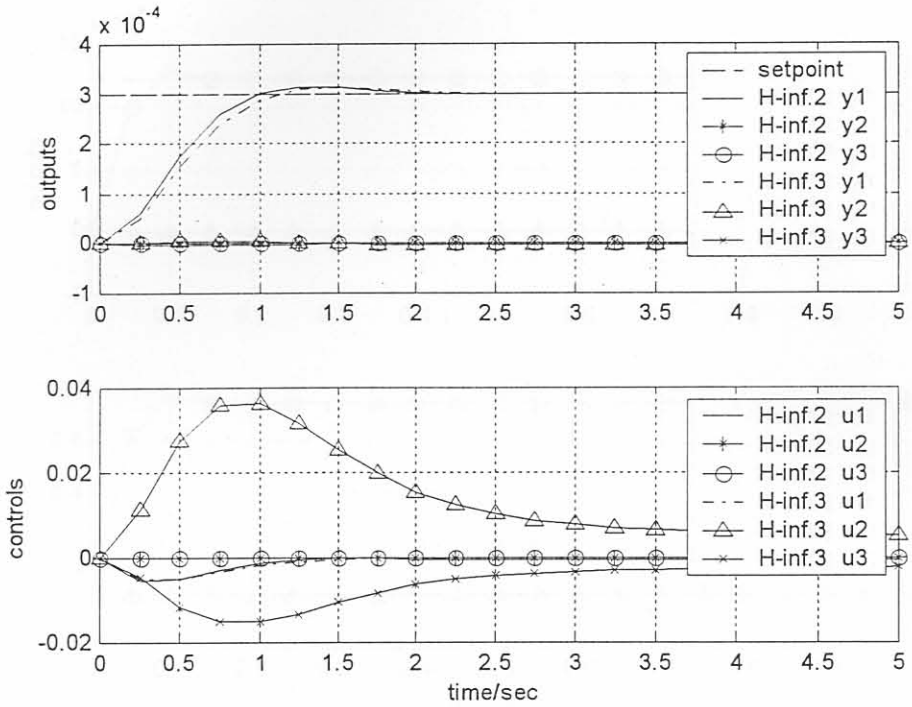

Figure 5.17: Closed loop simulation results of an H_∞ controller (H-inf.2) with the second linear model and an H_∞ controller (H-inf.3) with third linear model for the set point r = [3e-4 0 0] – (SI units apply).

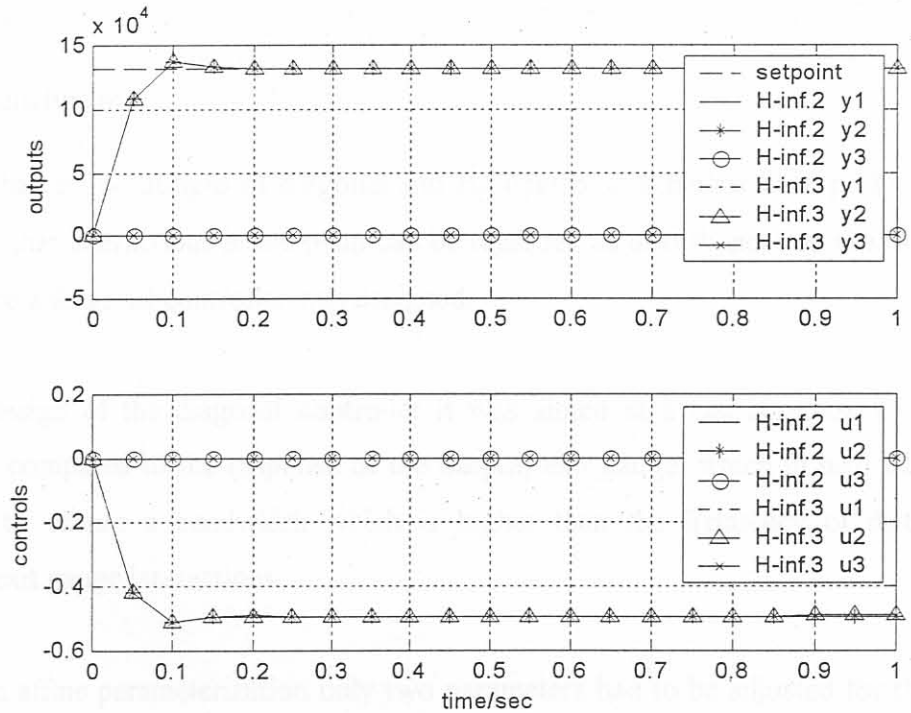

Figure 5.18: Closed loop simulation results of an H_∞ controller (H-inf.2) with the second linear model and an H_∞ controller (H-inf.3) with the third linear model for the set point r = [0 1.32e5 0] – (SI units apply).

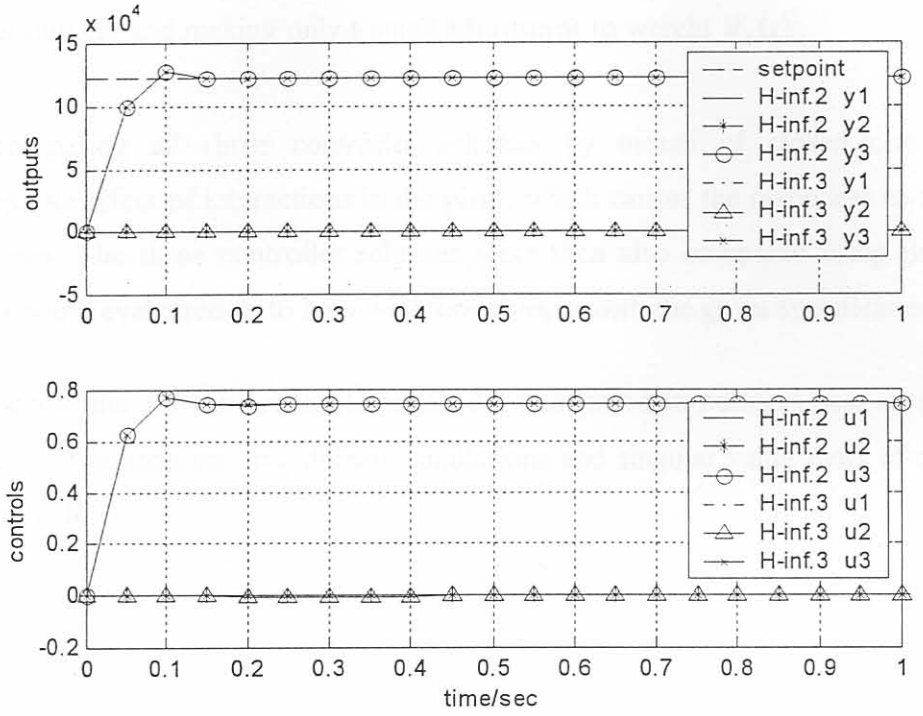

Figure 5.19: Closed loop simulation results of an H_∞ controller (H-inf.2) with the second linear model and an H_∞ controller (H-inf.3) with the third linear model for the set point r = [0 0 1.22e5] – (SI units apply).

5.7 Conclusion

In this chapter the designs of diagonal and H_∞ controller schemes were performed. It was assumed that interactions in the plant can be regarded as disturbances on the plant outputs, and hence a diagonal controller was designed.

In the design of the diagonal controller it was aimed at a fast response of the tension outputs, compared to the response of the output, exit gauge, which in turn had to be fast enough to ensure a bandwidth which is higher than the frequency of disturbance by tension/exit gauge interactions.

Using an affine parameterization only two parameters had to be adjusted for the tuning of the PID controller in the diagonal controller scheme. A desirable performance of the PI controllers in the diagonal control structure was obtained by pole placement design.

A diagonal H_∞ controller for the second linear model was designed by selecting weights on plant outputs and their errors appropriately. A second H_∞ controller was designed. This

design was based on the third linear model using the same weights as for the diagonal H_∞ controller initially and making only a small adjustment to weight $W_1(s)$.

When comparing all three controller schemes by means of closed-loop frequency responses, the effect of interactions in the plant, which causes the responses to deteriorate, can be seen. The three controller schemes were then also compared using time domain simulations and evaluated as to how well they comply with the given specifications.

The H_∞ controller for the second linear model was found to perform best according to a controller comparison on time domain simulations and singular value plots of closed loop transfer functions.